

TOPICAL REVIEW

## Surface defects in 4H-SiC: properties, characterizations and passivation schemes

To cite this article: Weiwei Mao *et al* 2023 *Semicond. Sci. Technol.* **38** 073001

View the [article online](#) for updates and enhancements.

### You may also like

- [Influence of the Surface Properties of SiC Particles on Their Codeposition with Nickel](#)  
M. Kaisheva and J. Fransaer
- [Photoluminescence in fluorescent 4H-SiC single crystal adjusted by B, Al, and N ternary dopants](#)  
Shi-Yi Zhuo, , Xue-Chao Liu et al.
- [Discrimination of dislocations in 4H-SiC by inclination angles of molten-alkali etched pits](#)  
Guang Yang, Hao Luo, Jiajun Li et al.

**PRIME**  
PACIFIC RIM MEETING  
ON ELECTROCHEMICAL  
AND SOLID STATE SCIENCE

HONOLULU, HI  
Oct 6–11, 2024

Abstract submission deadline:  
**April 12, 2024**

Learn more and submit!

**Joint Meeting of**  
The Electrochemical Society  
•  
The Electrochemical Society of Japan  
•  
Korea Electrochemical Society

## Topical Review

# Surface defects in 4H-SiC: properties, characterizations and passivation schemes

Weiwei Mao<sup>1,3</sup>, Can Cui<sup>1,\*</sup> , Huifan Xiong<sup>2,3</sup>, Naifu Zhang<sup>2,3</sup> , Shuai Liu<sup>2,3</sup>,  
Maofeng Dou<sup>3</sup>, Lihui Song<sup>2,3,\*</sup> , Deren Yang<sup>2,3</sup> and Xiaodong Pi<sup>2,3,\*</sup> 

<sup>1</sup> Key Laboratory of Optical Field Manipulation of Zhejiang Province, Department of Physics, Zhejiang Sci-Tech University, Hangzhou 310018, People's Republic of China

<sup>2</sup> State Key Laboratory of Silicon Materials & School of Materials Science and Engineering, Zhejiang University, Hangzhou 310027, People's Republic of China

<sup>3</sup> Institute of Advanced Semiconductors & Zhejiang Provincial Key Laboratory of Power Semiconductor Materials and Devices, ZJU-Hangzhou Global Scientific and Technological Innovation Center, Zhejiang University, Hangzhou 311200, People's Republic of China

E-mail: [cancui@zstu.edu.cn](mailto:cancui@zstu.edu.cn), [songlihui@zju.edu.cn](mailto:songlihui@zju.edu.cn) and [xdpi@zju.edu.cn](mailto:xdpi@zju.edu.cn)

Received 5 December 2022, revised 15 March 2023

Accepted for publication 12 May 2023

Published 8 June 2023



## Abstract

Silicon carbide (SiC) is a typical wide band-gap semiconductor material that exhibits excellent physical properties such as high electron saturated drift velocity, high breakdown field, etc. The SiC material contains many polytypes, among which 4H-SiC is almost the most popular polytype as it possesses a suitable band-gap and high electron saturated drift velocity. In order to produce 4H-SiC power devices with a high barrier voltage of over several thousand volts, the minority carrier lifetime of 4H-SiC single crystals must be carefully managed. In general, both bulk defects and surface defects in 4H-SiC can reduce the minority carrier lifetime.

Nevertheless, as surface defects have received less attention in publications, this study reviews surface defects in 4H-SiC. These defects can be classified into a number of categories, such as triangle defect, pit, carrot, etc. This paper discusses each one individually followed by the introduction of industrially feasible methods to characterize them. Following this, the impact of surface defects on the minority carrier lifetime is analyzed and discussed. Finally, a particular emphasis is put on discussing various passivation schemes and their effects on the minority carrier lifetime of 4H-SiC single crystals. Overall, this review paper aims to help young researchers comprehend surface defects in 4H-SiC single crystal material.

Keywords: silicon carbide, surface defects, characterizations, passivation schemes

(Some figures may appear in colour only in the online journal)

\* Authors to whom any correspondence should be addressed.

## 1. Introduction

Silicon carbide (SiC) is a typical wide band-gap semiconductor material suitable for power electronics due to its excellent electrical properties [1]. SiC material has many polytypes such as 4H-SiC, 6H-SiC, 3C-SiC, etc. Among these, 4H-SiC is the most used in electronic industry due to its proper band-gap and high electron saturated drift velocity. Hence, in this paper, we focus dominantly on 4H-SiC.

Among SiC power electronics, bipolar devices such as the thyristor and pin diode need a low on-resistance due to the conductivity modulation effect [2, 3]. But effective conductivity modulation requires a long minority carrier lifetime of the SiC wafer. To solve this problem, in recent years numerous studies have closely examined the minority carrier lifetime of SiC wafers. In the literature, Bergman and colleagues found that the minority carrier lifetime of a SiC wafer is associated with boron impurity [2, 4], small-angle grain boundaries [5], and some deep defects [6]. Moreover, the reciprocal of the minority carrier lifetime of a SiC wafer is convincingly demonstrated by Klein *et al* [7] and Danno *et al* [8] to be proportional to the concentration of  $Z_{1/2}$  defects [9]. In order to reduce  $Z_{1/2}$  defects and hence improve minority carrier lifetime, a two-step heat treatment (thermal oxidation followed by high temperature inert annealing (Ar)) has been reported [10]. After reducing  $Z_{1/2}$  defects to a small value, the minority carrier lifetime of 4H-SiC is predominately governed by an alternative recombination channel, notably surface recombination.

Some interesting discoveries about surface recombination have been reported. For instance, Masashi Kato *et al* [11] observed that the Si-face had a lower surface recombination velocity following chemical-mechanical polishing than the C-face. In addition, Mori *et al* [12] found that reactive ion etching increased the density of point defects in a 4H-SiC surface and hence increased its surface recombination velocity. Moreover, Mahadik *et al* [13] used the photoluminescence (PL) technique to investigate the minority carrier lifetime depth profile in a 4H-SiC epi-layer up to 140  $\mu\text{m}$  and found that surface defects have a significant impact on the minority carrier lifetime depth profile. Although surface recombination in 4H-SiC has been studied to some extent, the accurate measurement of surface recombination velocity, particularly its spatial distribution, in 4H-SiC and how various surface defects affect surface recombination have been less studied. As a result, it is essential to establish a framework of knowledge for the effects of, and characterization of surface defects.

After knowing about the surface defects in 4H-SiC, the next step is to passivate them. A number of passivation schemes have been developed with the goal of minimizing the detrimental effect of surface defects on the quality of the 4H-SiC material. In the literature, Pennington and Ashman [14] investigated  $\text{N}_2$  and NO passivation of the Si-face of 4H-SiC and found that N passivation was able to dramatically reduce the density of surface defect states in 4H-SiC. Furthermore, Ichikawa *et al* [15] also demonstrated that hydrogen from acidic solutions can passivate 4H-SiC surface defect states via

generating Si-H and C-H bonds. In addition, Su *et al* [16] studied sulfur (S) passivation of the SiC surface and found that the Si-S bonds and C-S bonds can reduce the density of surface defect states to a large extent. The above literature reports demonstrate that light elements like N, H, S are effective to passivate a 4H-SiC surface or interface. More discussion of the passivation phenomenon and mechanisms is available in section 5.

## 2. Surface defects and their formation mechanism

Currently, 4H-SiC wafers grown by the physical vapor transport (PVT) method still have a large number of surface defects. These defects affect the wafer's electronic parameters, reduce the yield of the subsequent device, and hinder the application of 4H-SiC in the field of power electronic devices. The triangle defect, pit, carrot defect, and surface step are the most common surface defects in a 4H-SiC wafer. Numerous investigations have demonstrated that the triangle defect and carrot defect are deadly defects that inevitably result in the device performance degrading or even failing. Surface steps have little influence on the performance of Schottky diode devices, but have a large detrimental influence on the performance of metal oxide semiconductor transistor (MOSFET) devices, resulting in an increase in leakage current and a decrease in breakdown voltage. A brief introduction of each typical surface defect is presented below.

### 2.1. Triangle defect

According to the experience analysis of epitaxial growth, the triangle defect evolves from the downfall particles at the surface of a 4H-SiC epilayer within the epitaxial growth process, as shown in figure 1(a). During epitaxial growth, downfall particles are easy to drop onto the surface of 4H-SiC due to the change of temperature, air flow and other growth conditions [17], and then they are encapsulated by subsequent epitaxial 4H-SiC to form a triangle defect. Downfall particles are typically located at the apex of the triangle region and its epitaxial products are attached to the fittings in the reaction chamber. Because 4H-SiC has strong high temperature resistance and corrosion resistance, downfall particles on the 4H-SiC surface cannot be completely removed. In the literature, the following methods are available to reduce the triangle defect: I. Improve the cleanness of the reaction chamber; II. Avoid the change of temperature, air flow and other important process parameters during the epitaxial growth; III. Shorten the epitaxial growth time as much as possible.

### 2.2. Pit

The pit is another typical surface defect and it is mainly located on the surface of the 4H-SiC epitaxial layer. A pit can be visualized by an atomic force microscope (AFM) and scanning electron microscopy (SEM). Two types of pits have been observed, which are made up of surface steps with the shape

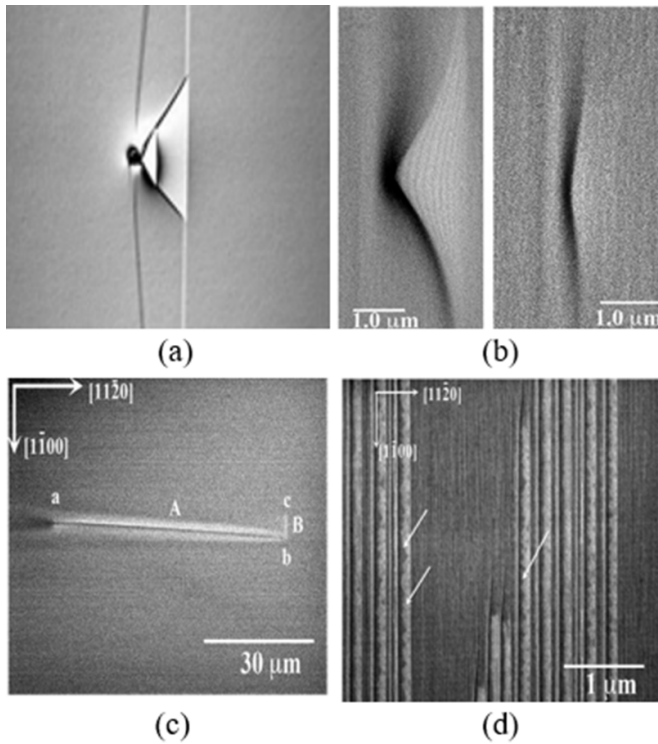


**Figure 1.** Various kinds of defect appearing in 4H-SiC wafers. (a) Triangle defect. (b) Pit. (c) Carrot defect. (d) Surface steps [29, 30]. Reproduced from [29, 30], copyright 2020, 2017, Elsevier, Microscopy.

of a letter I or a chevron bracket ‘<’ [18–20], as illustrated in figure 1(b). Further studies indicate that the pits with herringbone brackets and I marks consist of threading screw dislocation (TSD) and threading edge dislocation, respectively. In general, a pit can be formed during two processes: the first is initially formed during H<sub>2</sub> cleaning, and the second is grown during subsequent chemical vapor deposition (CVD) growth of the epitaxial layer. For the same wafer, a pit may vary in size and depth due to the different growth conditions as the flow rate of H<sub>2</sub> gas and CVD gas can be different, and the CVD growth temperature on the wafer surface can be uneven [21].

### 2.3. Carrot defect

A carrot defect is a major defect formed in the process of 4H-SiC epitaxial growth. The typical morphology of a carrot defect is shown in figure 1(c). It is named the carrot defect because it resembles a carrot in shape and is a surface defect caused by TSD dissociation during the growth of the epitaxial layer [22, 23]. A carrot defect typically consists of a stacking fault (SF) complex, of which the long length is TSD and SFs lay at both ends. The size of carrot defect is directly determined by the size of SFs [24]. It can form due to polishing scratches, TSD and substrate defects. Learning from its formation mechanism, carrot defects can be reduced

or eliminated by the following methods: I. Optimize the pre-etching process of the substrate to improve the atomic arrangement structure of the substrate surface; II. Optimize the growth conditions of epitaxial layer and reduce the decomposition rate of TSD.

### 2.4. Surface step

Surface step-like irregular wide terraces and high step structures are one of the common surface defects in 4H-SiC, as illustrated in figure 1(d). Surface steps are caused by substrate crystallization defects or scratches on the substrate surface, which are produced during H<sub>2</sub> etching [25]. The effect of surface step on 4H-SiC power electronic device has been studied [26–28]. It was reported that surface step has little effect on the performance of a Schottky barrier diode, but has evidently detrimental effect on a MOSFET, which will lead to the increase of the surface energy barrier and interface defect states, resulting in the decline of carrier mobility and minority carrier lifetime, and subsequently the performance of the MOSFET. To avoid surface step, two methods can be adopted: I. Reducing the growth temperature and rate; II. Improve the chemical mechanical polishing quality of the 4H-SiC substrate surface.

## 3. Electrical characterization methods for surface defects

In the literature, surface defects are generally characterized by scanning probe methods like SEM and AFM. Nevertheless, the electrical properties of surface defects must be revealed by some kinds of recombination characterization. In this section, four widely used methods, namely microwave photoconductivity decay ( $\mu$ -PCD), time-resolved PL (TRPL), scanning capacitance microscopy (SCM) and conductive atomic force microscopy (C-AFM) are introduced for the characterization of the electrical properties of surface defects. Before introducing these two methods in detail, a general concept of surface recombination is discussed below.

Typically surface recombination and bulk recombination contribute to the effective minority carrier lifetime. Suppose that the two recombinations occur separately,  $\tau_b$  refers to bulk lifetime,  $\tau_s$  refers to surface lifetime, then the effective minority carrier lifetime is

$$\frac{1}{\tau} = \frac{1}{\tau_b} + \frac{1}{\tau_s}, \quad (1)$$

where  $\tau$  is the effective minority carrier lifetime.

To understand surface recombination, it is essential to introduce the concept of surface recombination velocity. Surface recombination velocity is a generally used parameter to reflect the strength of surface recombination. Higher surface recombination velocity means more injected carriers have recombined on the surface, which seriously affects the device performance. Therefore, in the production of devices, it is vital

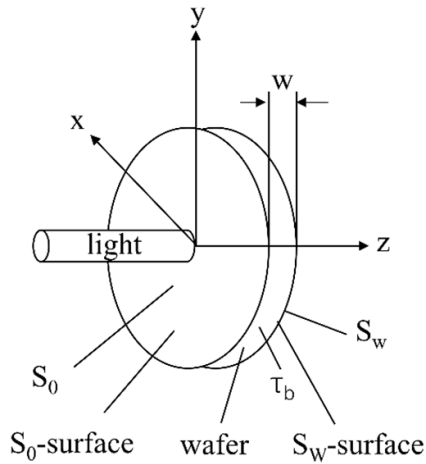


**Figure 2.** A schematic diagram explaining wafer parameters and an analysis model [31]. Reproduced from [31], copyright 1996, AIP Publishing.

to obtain a good and stable surface to reduce the surface recombination velocity. On the other hand, in some physical measurements, in order to eliminate the effect of metal probe injection, it is necessary to increase the surface recombination velocity to obtain more accurate measurement results.

Many methods have been developed to study effective minority carrier lifetime, such as PL decay and  $\mu$ -PCD. In both methods, a laser is applied to the material to create electron-hole pairs and then the laser radiation is turned off to monitor the signal decay curve. The decay curve is used to extract the effective minority carrier lifetime. Once the effective minority carrier lifetime is obtained, it can be seen from equation (1) that the corresponding surface recombination velocity can also be obtained, as long as the influence of bulk and surface recombination on the effective minority carrier lifetime is separated. Below are described two methods that are able to effectively separate the bulk recombination rate from the surface recombination velocity, to achieve the characterization of the electrical properties of surface defects.

### 3.1. $\mu$ -PCD

$\mu$ -PCD is a widely used method to measure the effective minority carrier lifetime and also the surface recombination velocity. Figure 2 shows the analytical model. Assuming that the thickness of the wafer is  $w$ , the bulk lifetime  $\tau_b$  is uniform along the  $z$  axis. The rate of excess carriers flowing into the front surface is  $S_0$ , the rate of excess carriers flowing into the back surface is  $S_w$ . Excess charge carriers are created in the wafer by pulsed light. Therefore, in this case, the generated minority carrier concentration  $\Delta n(z, 0)$  can be expressed by

$$\Delta n(z, 0) = g_0 \exp(-\alpha z), \quad (2)$$

where  $g_0$  is the carrier concentration at  $z = 0$  and  $\alpha$  is the absorption coefficient. The distribution of carriers in material follows the continuity equation thus:

$$\frac{\partial \Delta n(z, t)}{\partial t} = D \frac{\partial^2 \Delta n(z, t)}{\partial z^2} + G - \frac{\Delta n(z, t)}{\tau_b}, \quad (3)$$

where  $G$  refers to the generation rate of the minority carrier,  $D$  refers to the diffusion coefficient of the minority carrier,  $\Delta n(z, t)$  refers to the excess minority carrier concentration. The boundary condition is expressed by

$$D \frac{\partial \Delta n(0, t)}{\partial z} = S_0 \Delta n(0, t), \quad (4)$$

$$D \frac{\partial \Delta n(w, t)}{\partial z} = -S_w \Delta n(w, t). \quad (5)$$

The average photoconductivity change  $\sigma(t)$  is then given by:

$$\sigma(t) = \frac{q\mu}{w} \int_0^w \Delta n(z, t) dz, \quad (6)$$

where,  $\mu$  is the mobility of carrier and  $q$  is elemental charge.

The relationship between  $\tau_b$ ,  $S_0$  and  $S_w$  can be analyzed by fitting the decay curve of photoconductivity. As shown in figure 3, the vertical intercept of the asymptote of the decay curve is significantly dependent on  $S_0$  and  $S_w$  and is independent of  $\tau_b$ . Therefore, the same or different wavelengths of light can be used to illuminate the  $S_0$  or  $S_w$  surfaces to generate different carrier diffusion processes [31], thus two different intercepts can be obtained, and subsequently the unique  $S_0$  and  $S_w$  can be determined. It is worth noting that the pulse width of the incident light is assumed to be infinitesimal in this method. Nevertheless, actual light pulses have a finite width. Fortunately, experiments show that light pulse width less than 100 ns has almost no effect on the photoconductivity decay curve. Additionally, the model assumes that the light intensity distribution in the wafer is a simple exponential, so the effect of multiple reflections is not considered.

The shortcoming of this method is that it can only give the average value of the surface recombination velocity of the sample containing a certain surface defect without revealing its shape, but the advantage is that the equipment for this method is generally simple and cheap.

### 3.2. TRPL

The PL decay method is another method that is able to demonstrate the spatial surface recombination property of surface defects. The PL decay method includes phase shift and TRPL. The phase shift method assumes that the PL signal is exponentially attenuated. However, if the decay is non-exponential, the phase shift method will produce inaccurate results. The TRPL method can avoid this problem and therefore is predominantly adopted in industry and lab [32]. Literature reports that the TRPL method provides detailed characterization of non-exponential decay and is sensitive enough to measure the lifetime at a very low injection level. Furthermore, this technique is non-contact and can be applied to very small sample.

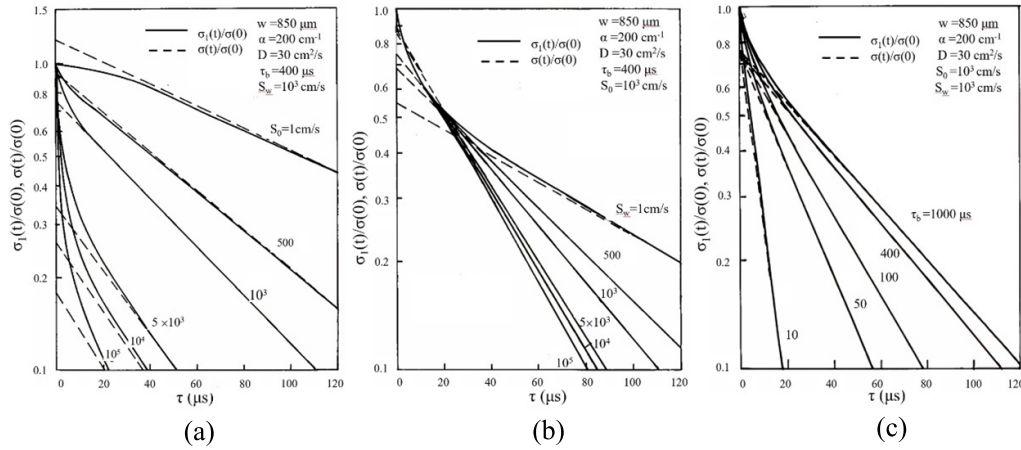


**Figure 3.** The normalized photoconductivity decay for various values of  $\tau_b$ ,  $S_0$ ,  $S_w$  [31]. Reproduced from [31], copyright 1996, AIP Publishing.

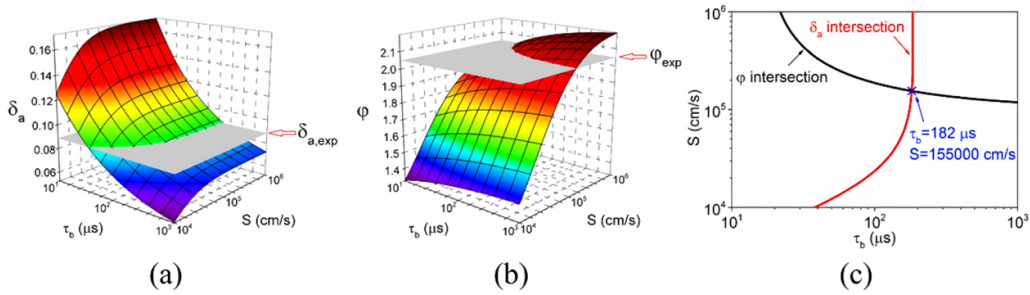


**Figure 4.** (a)  $\delta$  mapping and (b)  $\varphi$  mapping for calculating  $\tau_b$  and  $S$ . The two grey planes in (a) and (b) will intersect the mappings of  $\delta$  and  $\varphi$ , resulting in two curves as illustrated in (c) [33]. Reproduced from [33], copyright 2014, AIP Publishing.

To understand the mechanism of the TRPL method, it is essential to pre-understand the properties of the emitted photon flux from the radiative recombination in a material. The emitted photon flux depends on two factors. One is the rate of photon production, which is determined by the radiative recombination rate of photogenerated or electrically generated carriers. The other is the escape rate of the photons, which depends on the reabsorption of the photons as well as the optical properties of the sample. For simplicity, the properties of the sample are assumed to be laterally homogeneous, which allows a one-dimensional description of the luminescence emission. In this case, the emitted luminescence photon flux per wavelength interval and per solid angle is given by

$$\Phi_{\text{emit}}(\lambda) = SR(\lambda) \int_0^w r_{\text{ph}}(\lambda, z) f_{\text{esc}}(\lambda, z) dz, \quad (7)$$

where,  $r_{\text{ph}}(\lambda, z)$  refers to the photon production rate and  $f_{\text{esc}}(\lambda, z)$  refers to the photon escape rate. Considering the efficiency of the detector and the optical loss along the optical path from the semiconductor interface to the detector, these two factors consist of the spectral response of the detection system and are expressed as  $SR(\lambda)$ .  $\lambda$  refers to the wavelength

of light,  $W$  refers to the thickness of the sample and  $z$  refers to the position ranging from 0 to  $w$ .

The detailed method to extract the spatial surface recombination velocity from TRPL is described below. When the wafer is thick enough, the back surface recombination velocity can be considered to be zero. In this case, two beams of light with different excitation wavelengths can be used to irradiate the sample. The two PL ratios obtained in the steady state can be defined as  $\varphi$ , and the ratio in the transient state can be defined as  $\delta$  (as shown in figure 4). In this case,  $\varphi$  and  $\delta$  can be measured experimentally (shown in the gray area), and two curves of  $S$  and  $\tau_b$  can be obtained by fitting the relationship between  $\varphi$ ,  $\delta$ ,  $\tau_b$ , and  $S$ . The intersection point as shown in figure 4(c) indicates the bulk lifetime and the surface recombination velocity of each point, respectively [33].

In the case where the sample is thin and the rear surface recombination velocity is not zero, according to the PL intensity measured locally on the wafer, the luminescence images obtained by different optical short-pass filters can be used to extract the recombination parameters expressed by  $\tau_b$  ( $S_0$ ,  $S_w$ ) (as shown in figure 5). Surface recombination velocity and bulk lifetime are then obtained by the intersection points of three fitting graphs through three measurements [34].

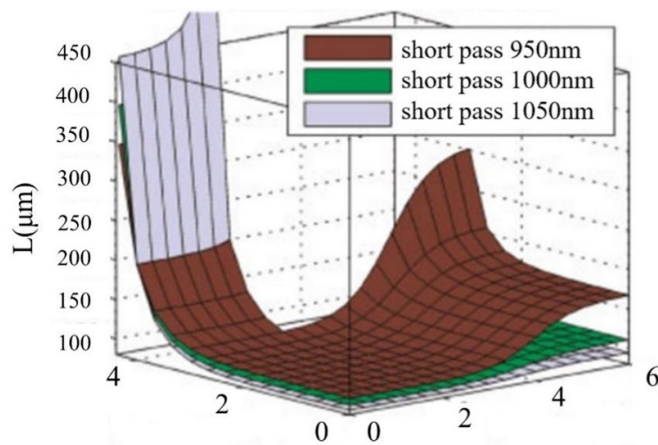


**Figure 5.** A local PL intensity measured on a silicon wafer [34]. Reproduced from [34], copyright 2010, John Wiley and Sons.

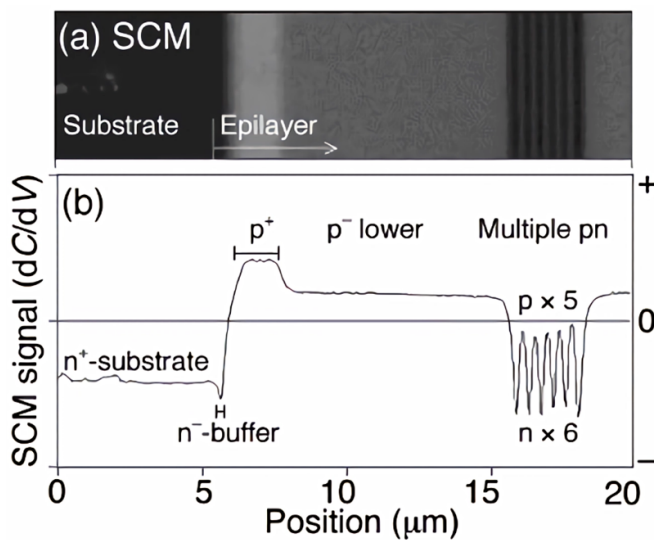


**Figure 6.** Cross-sectional SCM ( $dC/dV$ ) image and (b) its line profile [38]. Reproduced from [38], copyright 2002, IOP Science.

### 3.3. SCM

The principle of SCM is to coat the probe of AFM with a conductive coating and scan the semiconductor surface. A two-dimensional visual distribution of charge carriers may be produced by recording the change in radio frequency amplitude signal caused by the local change in capacitance between the sample and the metal probe [35, 36]. SCM is commonly used in combination with atomic force microscopy. Using this technique, precise measurements may be made without causing any harm to the material. The morphology and electrical properties can both be obtained [37].

As shown in figure 6, after observing the device morphology through AFM, no special feature was observed, the SCM image originates from local electrical properties. The  $0.2\ \mu\text{m}$ -thick n-type layer and  $0.3\ \mu\text{m}$ -thick p-type layer in the multiple pn-junction were clearly resolved [38].

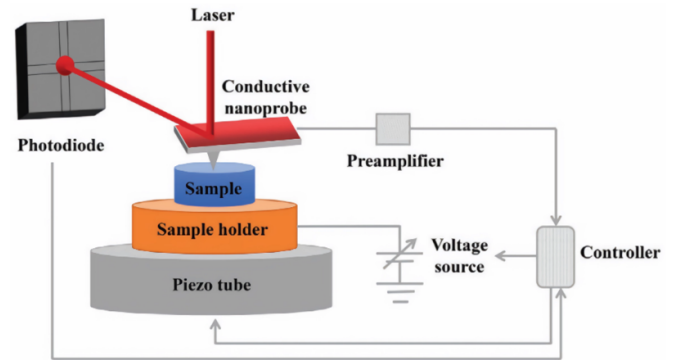


**Figure 7.** Diagram of the principles of C-AFM [44]. Reproduced from [44], copyright 2019, John Wiley and Sons.

Fiorenza *et al* [39] evaluated the lateral homogeneity of the active donor at the  $\text{SiO}_2/\text{SiC}$  interface at the nanoscale using plan-view SCM images, which can help observe current transmission in the channel region of  $\text{SiO}_2/\text{SiC}$ . Doi *et al* [40] measured differential capacitance through SCM and observed carrier density distribution and loss region diffusion in the p-type and n-type regions of operating power devices. Fiorenza *et al* [41] observed the triangular space charge distribution around threading dislocations (TDs) and analyzed its effect on the dielectric breakdown of the 4H-SiC epitaxial layer.

### 3.4. C-AFM

The principle of C-AFM is to characterize the electrical properties by measuring the current between the probe and the substrate [42]. As shown in figure 7, when the conductive probe is swept across the surface of the sample, a bias is applied to form a loop between the probe, sample and substrate, that generates a current. Once the current changes, the electrostatic force between the probe and the sample causes the cantilever to bend to different angles, thus distinguishing the spatial differences of current on the sample surface by drawing a two-dimensional plot [43].

C-AFM can detect charge transfer and electrical characteristics by measuring the current under short circuit condition, and judge the influence of different defects on the electrical conductivity of the sample by the size of the current [45, 46]. It can also distinguish differences within grains and at grain boundaries by nanoscale resolution. Eriksson *et al* [47] conducted local stress tests on  $\text{SiO}_2/3\text{C-SiC}$  interfaces through C-AFM, and studied the influence of different defects on the breakdown electric field of devices. They found that step-bunching of different heights on the surface of 3C-SiC would lead to the increase of local electric field strength, resulting in the breakdown of devices. Fiorenza *et al* [41] performed nanoscale electrical characterization of TDs through C-AFM and found that there were always TDs at the breakdown position of the device.

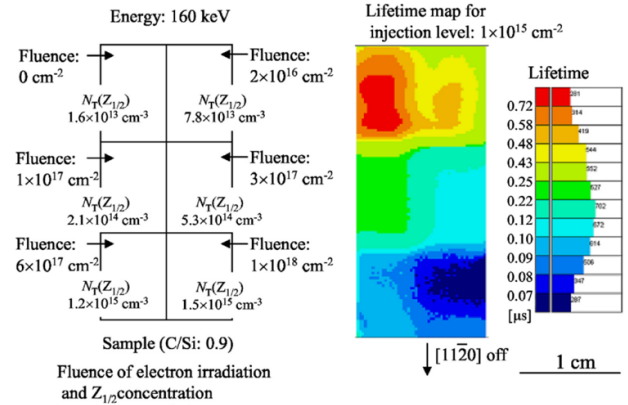
## 4. Effects of surface defects on minority carrier lifetime

### 4.1. Effect of surface recombination on the effective lifetime at low $Z_{1/2}$ concentration

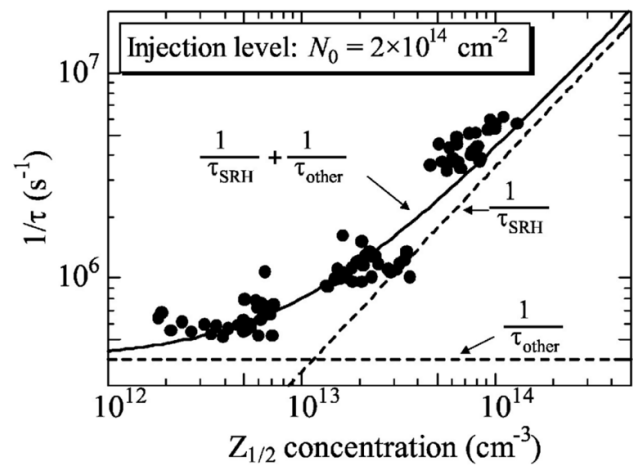
Minority carrier lifetime is an important parameter that reflects the electrical quality of 4H-SiC material. Minority carrier lifetime can be affected by both bulk defects and surface defects. For bulk defects, recombination centers with defect energy levels at 0.65 eV, 1.5–1.6 eV and 0.15–0.17 eV have been reported [48]. The 0.15–0.17 eV trap is thought to be caused by Ti [6], the 0.65 eV trap is the well-known negative-U centers  $Z_{1/2}$  [49], also identified as carbon vacancy [50], and 1.5–1.6 eV trap is commonly known as  $\text{EH}_6/\text{EH}_7$  trap [51], which some researchers have linked to another charge state of carbon vacancy [6]. In further study of the lightly doped n-type 4H-SiC epitaxial wafers of different thickness, Danno *et al* found that the lifetime of the epitaxial layer is mainly controlled by the  $Z_{1/2}$  defect [8, 52]. As shown in figure 8, Danno *et al* found that the SRH recombination caused by the  $Z_{1/2}$  defect controlled the minority carrier lifetime when the concentration of  $Z_{1/2}$  is higher than  $10^{13} \text{ cm}^{-3}$  [53, 54]. For a  $Z_{1/2}$  concentration below  $10^{13} \text{ cm}^{-3}$ , the measured minority carrier lifetime does not depend on the  $Z_{1/2}$  concentration, indicating that other competing recombination channels determine the minority carrier lifetime of the sample, possibly from the surface or interface defects.

Other competing processes that may control the minority carrier lifetime have been studied by researchers. For instance, Klein *et al* [55] grew 4H-SiC epitaxial layers with a low concentration of  $Z_{1/2}$  defect, and analyzed the bulk, surface, and interface recombination by comparing different recombination mechanisms at different temperatures. By comparing the measurements with simulations of temperature-dependent surface and bulk recombination rates, it is found that thermal activation of recombination rates increases at lower temperatures and surface capture prevails over diffusion. Typically the temperature dependence of the minority diffusion coefficient is compatible with the recombination rate at high temperatures, and this coefficient can only be influenced by surface recombination, independent of bulk defects. From these results, it can be determined that for low  $Z_{1/2}$  4H-SiC samples, the surface recombination determines the minority carrier lifetime.

Furthermore, Kimoto *et al* [56] measured the change of minority carrier concentration with the depth of epitaxial layer by the microwave photoconductivity method, as shown in figure 9. When the thickness of the epitaxial layer is small (figure 9(a)), 15% of carriers are recombined on the surface within 0.5  $\mu\text{s}$ . Within this time range, the minority carrier lifetime is mainly controlled by the recombination both from the surface and substrate. After 5  $\mu\text{s}$ , about 98% of the generated carriers have been recombined, which is consistent with the bulk lifetime of the epitaxial layer. When the thickness of the epitaxial layer is large (figure 9(b)), bulk recombination has



(a)



(b)

**Figure 8.** (a)  $Z_{1/2}$  concentration profile within a 4H-SiC epilayer that resulted from electron irradiation. (b) Subsequent lifetime map after annealing at 950 °C. (c) Curve fitting between the inverse of the measured lifetime and  $Z_{1/2}$  defect concentration [8]. Reproduced from [8], copyright 2007, AIP Publishing.

little effect on the excess carrier concentration distribution. Within 0.5  $\mu\text{s}$ , the recombination of carriers at the substrate only accounts for 1%–2% of the total recombined carriers, and the influence of surface recombination dominates the total recombination. By fitting the decay curves of excess carriers at different surface recombination velocities, as shown in figure 10, it is found that when the surface recombination velocity is greater than  $10^3 \text{ cm s}^{-1}$ , the lifetime of the sample is significantly reduced, indicating that the surface recombination is the dominant lifetime killer in this case.

### 4.2. Effect of various surface defects on surface recombination ability

Surface recombination is an important component of minority carrier lifetime. But how surface recombination is determined



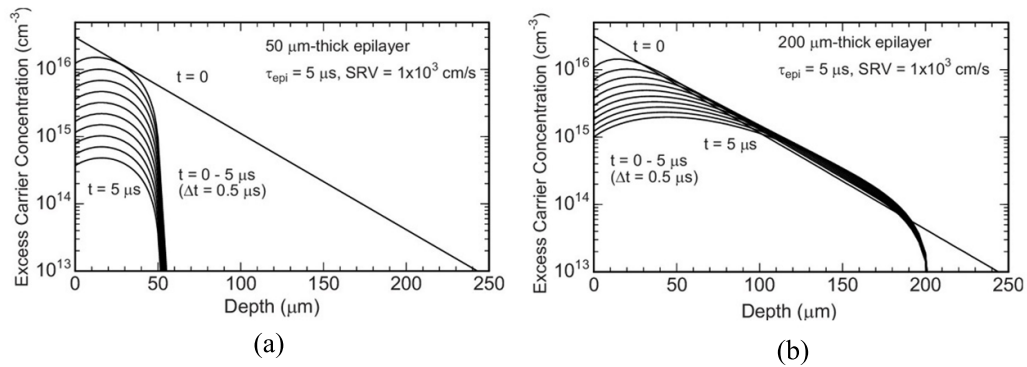


**Figure 9.** Excess carrier concentration depth profile within the 4H-SiC epilayer at different excitation times. The thickness of the epilayer is (a) 50 μm and (b) 200 μm [56]. Reproduced from [56], copyright 2010, AIP Publishing.

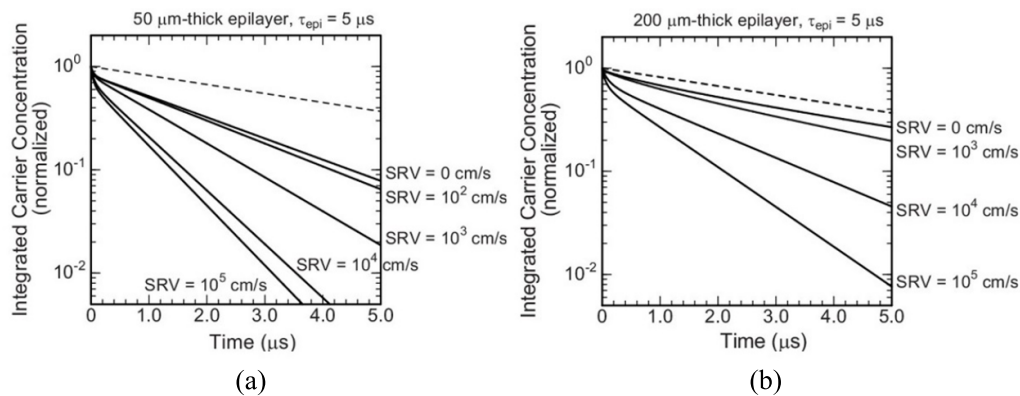


**Figure 10.** Excess carrier concentration decay profile with time. A bulk lifetime equal to 5.0 μs was assumed for the epilayer thickness of (a) 50 μm and (b) 200 μm [56]. Reproduced from [56], copyright 2010, AIP Publishing.

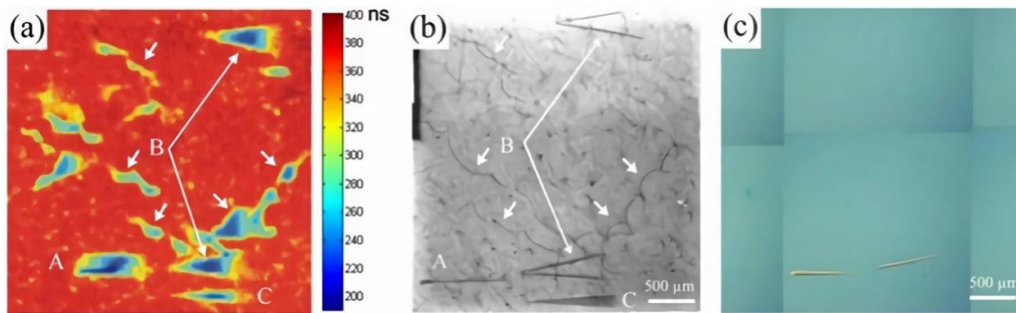


**Figure 11.** (a) Minority carrier lifetime spatial mapping of the sample. (b) Synchrotron white beam x-ray topography (SWBXT) image of the sample. (c) Optical image of the sample [60]. Reproduced from [60], copyright 2009, AIP Publishing.

is another significant question. The literature reports that surface defects such as the carrot defect, triangle defect, pit and surface step can dramatically influence the surface recombination ability of 4H-SiC material.

First, the carrot defect can cause severe surface recombination. As revealed in figure 11, via comparing the minority carrier lifetime mapping with synchrotron white beam x-ray topography, it is observed that carrot defects cause serious lifetime loss in some localized regions. In figure 11(a), the area without carrot defect has a minority carrier lifetime of 390 ns,

whereas the minority carrier lifetime at carrot defects reduces to 220 ns. Second, pits can also lead to localized enhanced surface recombination. In figure 12, the region of pits demonstrates an evident localized reduction of minority carrier lifetime. These pits have similar morphology, and become darker in the upward direction, which suggests that they are lying in the basal plane. Further study demonstrated that the pits consist of in-grown SFs like single-layer Shockley SFs as reported in [57]. Third, the triangle defect is also able to reduce the minority carrier lifetime of 4H-SiC material [58]. Figure 13(a)

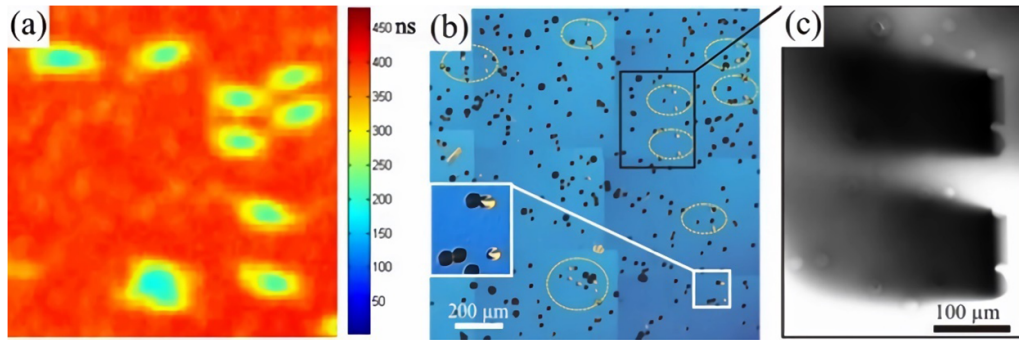


**Figure 12.** (a) Minority carrier lifetime spatial mapping of the sample (b) optical image of the sample after KOH etching. (c) Panchromatic cathodoluminescence (CL) image of the region marked with box in (b) [60]. Reproduced from [60], copyright 2009, AIP Publishing.

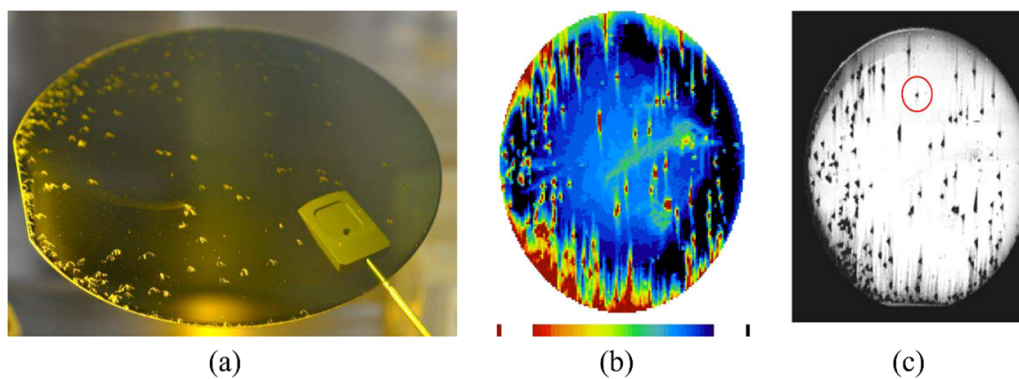


**Figure 13.** (a) Optical image of an SiC wafer with many triangular defects, (b) its minority carrier lifetime mapping, and (c) its PL mapping [59]. Reproduced from [59], copyright 2018, IOP Science.

reveals an optical image of an SiC wafer with many triangle defects. Its lifetime mapping and PL mapping are illustrated in figures 13(b) and (c) [59]. It is evidently demonstrated that the region of triangle defects has lower minority carrier lifetime and PL counts, particularly at the edge of the SiC wafer.

## 5. Passivation schemes for surface defects

Surface defects can lead to severe recombination in a 4H-SiC surface and cause other problems like leakage current and low breakdown voltage, resulting in a significant degradation of the performance of power electronic devices. Therefore, it is essential to find good methods to passivate surface defects. The recombination ability of various surface states dominantly comes from its dangling bonds or impurity contamination within certain surface defects. Hence, light element termination of dangling bonds or impurity atoms could be a good route to passivate surface defects.

### 5.1. N passivation

N is an useful element to passivate surface defects in 4H-SiC. In the literature, Pennington and Ashman [14] reported

a study of N passivation on a Si surface in 4H-SiC. Significant improvements are found in various parameters after N passivation treatment. In detail, the interface trap density is reduced, the mobility of carriers is increased, and the stability of the device is improved. Moreover, Chung *et al* [61] reported that after N passivation, the density of surface defect states declines for those with defect energy close to the conduction band and increases for those with defect energy close to the valence band. They speculated that the passivation of carbon atoms and carbon clusters by N may cause the defect energy levels to shift from the upper half level in the band-gap to the lower level close to the valence band. Furthermore, massive nitrogen atoms are observed to locate at the SiC/SiO<sub>2</sub> interface [62]. Further results demonstrate that N can passivate the suspended bond (as shown in figure 14) on the 4H-SiC surface to form Si–N bonds during oxidative annealing. Simultaneously, a small number of C–N bonds were formed, but Chung *et al* believed that C–N bonds that appeared near the interface could not play a role in passivation. Jamet *et al* [63] found more evidence that the C–N bond was more likely to remove carbon from the interface, whereas the Si–N bond is considered to play a key role for SiC/SiO<sub>2</sub> interface passivation. Akiyama *et al* [64]. Studied the effect of the density of N atom at the 4H-SiC/SiO<sub>2</sub> interface after N passivation of the interface state. In figure 15, when the concentration of N on the Si-face is larger

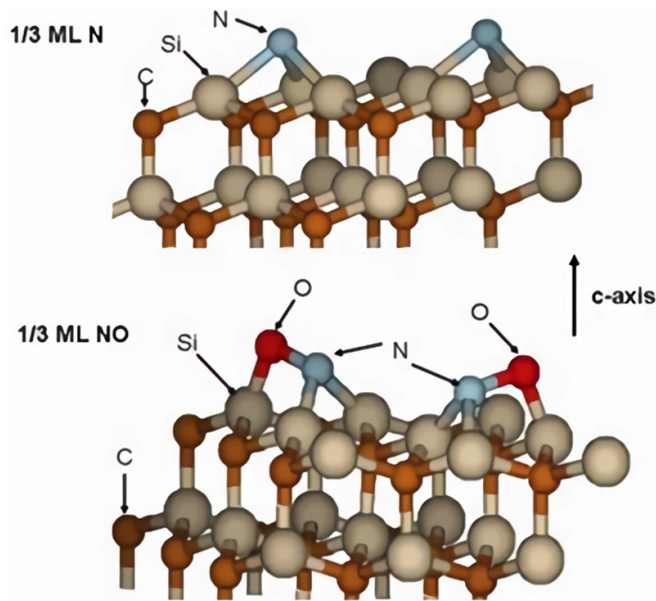


**Figure 14.** A schematic diagram to show the N passivation of the Si face in 4H-SiC material [14]. Reproduced from [14], copyright 2007, Trans Tech Publications Ltd.

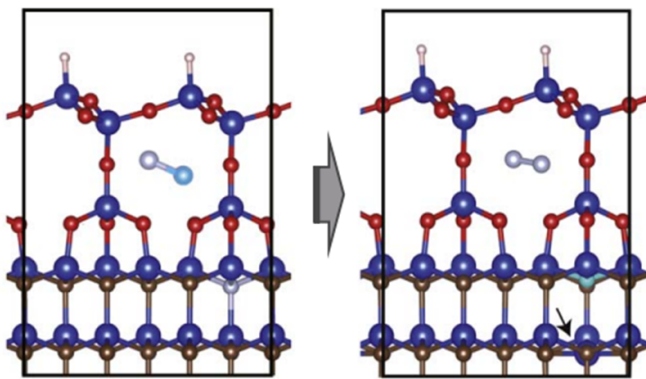


**Figure 15.** Schematics of structural change for the desorption of N atoms as an  $N_2$  molecule on the Si-face [64]. Reproduced from [64], copyright 2022, JSAP.

than  $3 \times 10^{14} \text{ cm}^{-2}$ , an N atom will replace an O atom in the NO molecule, and form an  $N_2$  molecule and precipitate out.

Kimoto *et al* [65] investigated the additional benefits of N passivation after conventional dry oxide plus deposition oxide passivation on an n-type 4H-SiC surface. Dry oxide is formed by placing the sample in pure  $O_2$ , growing it at  $1150^\circ\text{C}$ , and then annealing it in ambient argon for 30 min. Deposition oxide is then formed by plasma-enhanced CVD at  $400^\circ\text{C}$ , followed by nitridation via nitric oxide (NO) annealing at  $1300^\circ\text{C}$  for 30 min [66]. The thickness of dry oxide is about 10 nm, and the thickness of deposition oxide is about 12 nm. To demonstrate the additional benefits of N passivation, photoconductivity decay curves of 4H-SiC epitaxial wafers with different passivation schemes are illustrated in figure 16. It reveals that the passivation effect of dry oxide is slight, but

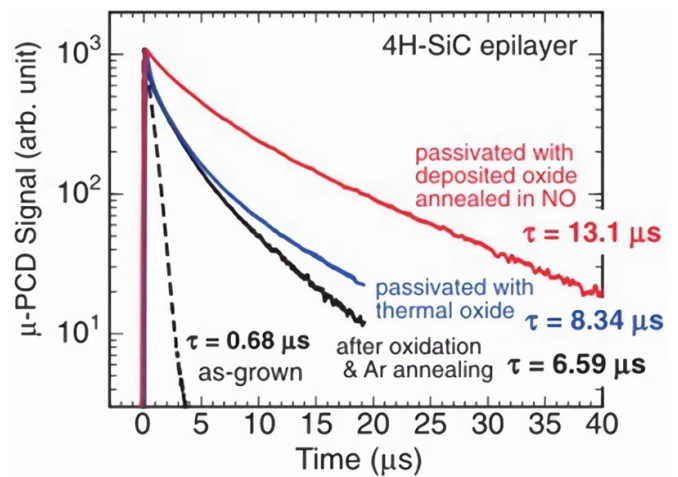


**Figure 16.** The effective minority carrier lifetime of the samples with different passivation schemes [65]. Reproduced from [65], copyright 2009, JSAP.

the minority carrier lifetime of the sample can be significantly increased to  $13.1 \mu\text{s}$  after N passivation.

## 5.2. H passivation

Hydrogen passivation via wet chemistry or thermal gas annealing is another effective method to passivate 4H-SiC surfaces [67–69]. The mechanism is due to the hydrogen termination of silicon or carbon dangling bonds leading to the reduction of electro-active surface defect states. It is reported that the Si–H and C–H bonds are located below the valence band and the antibonding states are located above the conduction band [70]. Because the basal planes of 4H-SiC are structurally equivalent to silicon and diamond (111) surfaces, some studies have attempted to passivate hexagonal 4H-SiC surfaces by hydrogenation [71–73]. Early attempts focused on hydrogenation of the Si-terminated surface, but OH groups were left on the 4H-SiC surface after hydrogenation [74]. Additionally, Lin *et al* [75] processed 6H-SiC(0001) in hydrogen plasma, which successfully reduced surface recombination. Detailed analysis indicated the reduction of the surface recombination was due to hydrogenation as the  $\text{SiO}_x$  signal was not detected by x-ray photo-electron spectroscopy (XPS).

Elsbergen *et al* [76] achieved surface reconstruction by exposing 6H-SiC (0001) and 3C-SiC (001) faces to hydrogen atoms in an ultra-high vacuum at a high temperature. Compared to untreated surfaces, the treated surfaces exhibit significantly reduced oxygen uptake, which was regarded as evidence of successful surface hydrogenation. In addition, Ichikawa *et al* [15] measured the effective lifetime of 4H-SiC samples in various aqueous solutions. It is found that low pH values have a greater passivation effect on minority carrier lifetime as it provides more hydrogen. Besides, the impact of hydrogenation depends on the elements to be passivated. For instance, as shown in figure 17, when excited on the n-type sample Si-face, the  $\mu$ -PCD decay curve of the sample

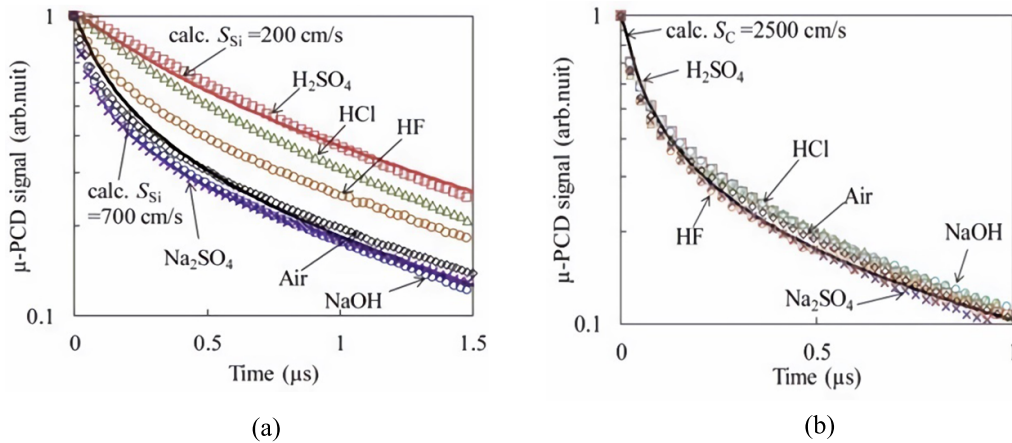


**Figure 17.**  $\mu$ -PCD signals for the Si-face and C-face of an n-type 4H-SiC sample in air or in aqueous solutions [15]. Reproduced from [15], copyright 2018, ECS.

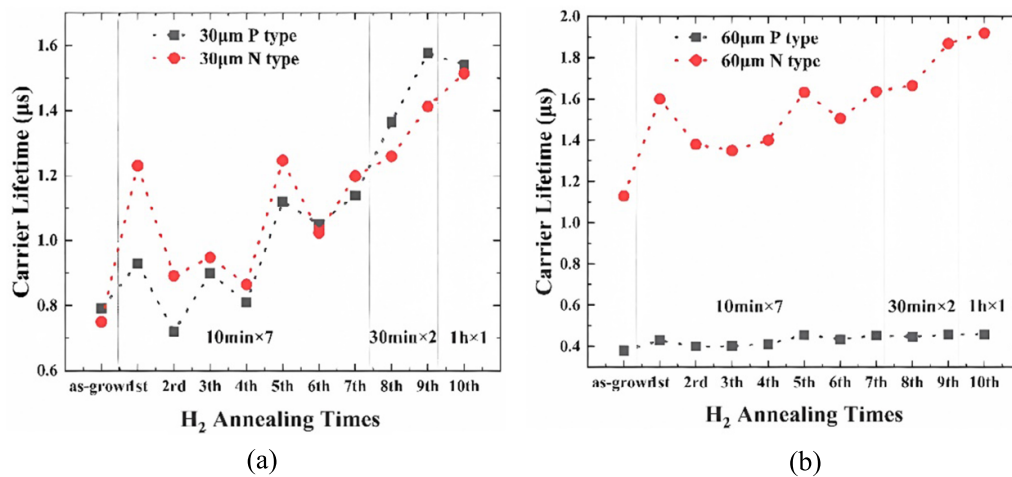


**Figure 18.** Measured carrier lifetimes in 30  $\mu\text{m}$  (a) and 60  $\mu\text{m}$  (b) N- and P-type 4H-SiC epitaxies after  $\text{H}_2$  annealing [77]. Reproduced from [77], copyright 2021, IEEE.

immersed in acidic solution is gentler than that in other conditions, which indicates that the silicon dangling bonds are passivated by hydrogen. Nevertheless, when the incident laser is on the C-face, the  $\mu$ -PCD signal is almost independent of the immersion solution, which indicates that the carbon dangling bonds are not easily passivated by hydrogen. The above results suggest that hydrogen in the acidic solution passivates the surface defect states on the Si-face but has no effect on the C-face. Also, it is worth noting that the passivation effect gradually decreases in air with time at room temperature, so the passivation of the acidic solution cannot be used for the manufacturing process of electronic devices. Zhang *et al* [77] compared the effect of different times of hydrogen annealing on the minority carrier lifetime of 4H-SiC with different thicknesses and different doping types by  $\mu$ -PCD. In figure 18, they found that the minority carrier lifetime of all samples increased or decreased due to the instability of hydrogen passivation. After the 10th hydrogen passivation, the minority carrier lifetime tended to increase.

### 5.3. Other passivation methods

Sulphur (S) passivation is another effective method to passivate a 4H-SiC surface. In the literature, Su *et al* [16] studied the S passivation of 3C-SiC thin films and compared the passivation effects achieved by different solutions, as shown in table 1. The samples were characterized by XPS spectroscopy, and the results are shown in figure 19. The Si 2p spectra of the three samples showed S 2p peaks, and the XPS spectra of C 1s as well showed S 2p peaks, which indicated the formation of Si-S bonds and C-S bonds. Moreover, because of the addition of S powder in solution 2, the concentration of  $\text{S}^{2-}$  is higher, leading to a higher peak value of S 2p, which indicates the passivation effect of S on 3C-SiC is better.

Phosphorus (P) is also a useful element to passivate a 4H-SiC surface. Figure 20 demonstrates that  $\text{POCl}_3$  annealing can enhance the minority carrier lifetime of the sample from 0.5 to 3  $\mu\text{s}$ . In order to investigate whether  $\text{POCl}_3$  annealing affected the surface recombination or not, the  $\text{SiO}_2$  layer of

**Table 1.** The conditions for S passivation schemes.

	The solution recipe	PH condition	Temperature (°C)	Time (minutes)
1 <sup>#</sup>	(NH <sub>4</sub> ) <sub>2</sub> S(0.33 mol l <sup>-1</sup> ) +NH <sub>3</sub> ·H <sub>2</sub> O (2.4 mol l <sup>-1</sup> )	pH > 7	60	30
2 <sup>#</sup>	(NH <sub>4</sub> ) <sub>2</sub> S(0.33 mol l <sup>-1</sup> ) +NH <sub>3</sub> ·H <sub>2</sub> O (2.4 mol l <sup>-1</sup> ) + S powder(2.1 g)	pH > 7	60	30
3 <sup>#</sup>	(NH <sub>4</sub> ) <sub>2</sub> S (0.33 mol l <sup>-1</sup> ) +NH <sub>3</sub> ·H <sub>2</sub> O (2.4 mol l <sup>-1</sup> ) + HF	pH = 7	60	30

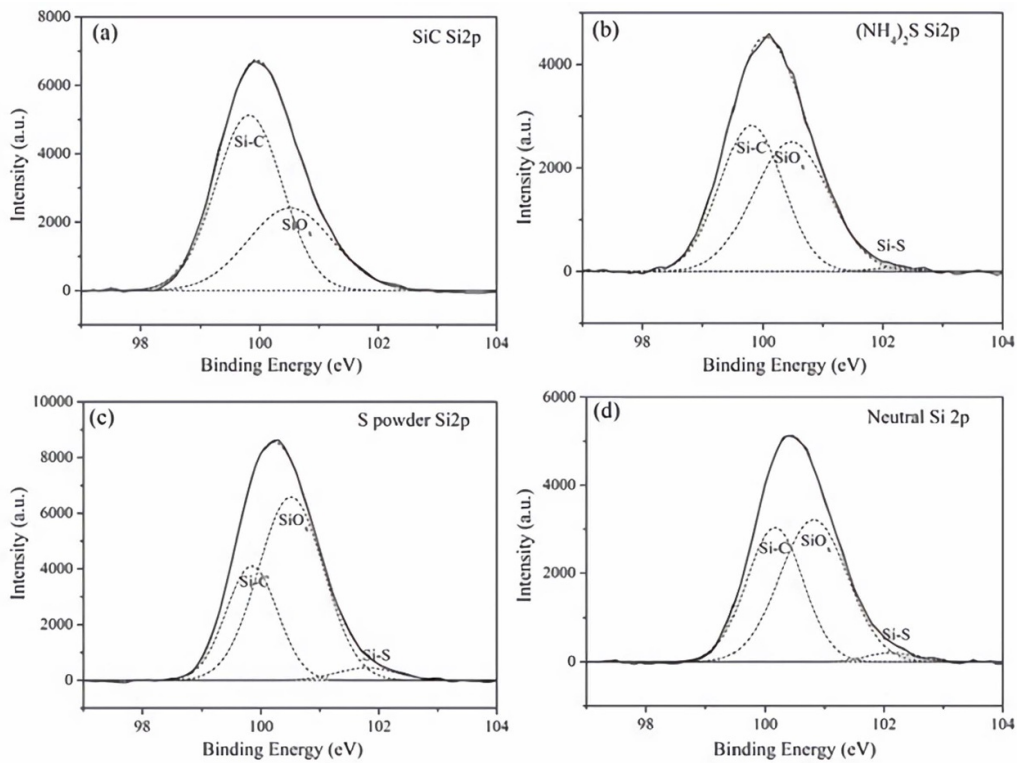


**Figure 19.** XPS spectra showing Si 2p core-level (a) Silicon 2p spectra in non-passivated sample; (b)–(d) Silicon 2p spectra with sample in passivation solution 1<sup>#</sup>, 2<sup>#</sup>, 3<sup>#</sup> [16]. Reproduced from [16], copyright 2019, Elsevier.

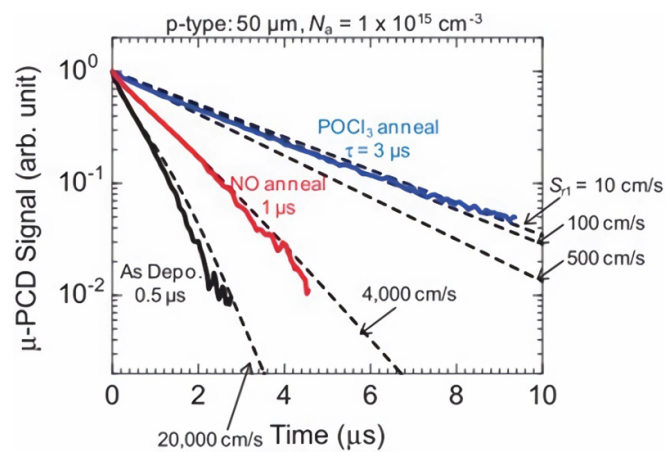


**Figure 20.** Effect of NO or POCl<sub>3</sub> annealing on photo-conductance decay curves of the samples [78]. Reproduced from [78], copyright 2016, JSAP.

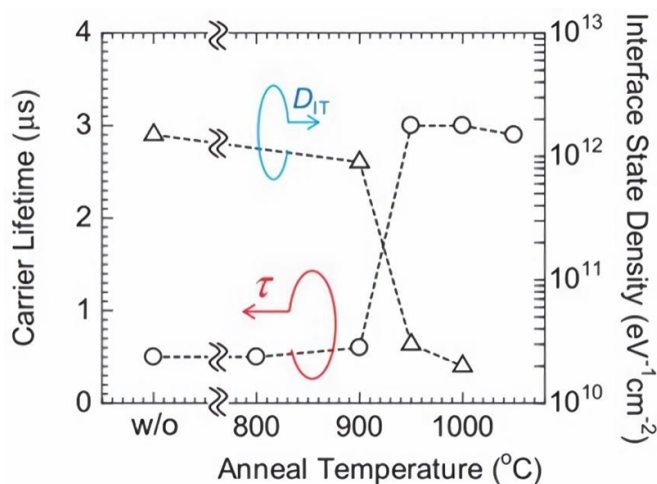


**Figure 21.** Minority carrier lifetimes of the samples after  $\text{POCl}_3$  annealing at different temperatures. Interface defect state densities are also shown via the measurement of high (1 MHz)–low C-V technique [78]. Reproduced from [78], copyright 2016, JSAP.

the sample was removed by an HF solution and subsequently a new layer of  $\text{SiO}_2$  was deposited by PECVD. The result demonstrated that with the new layer of  $\text{SiO}_2$ , the lifetime of the sample was only  $0.5 \mu\text{s}$ , which suggested  $\text{POCl}_3$  annealing did indeed improve surface passivation. Furthermore, minority carrier lifetime of the p-type 4H-SiC epitaxial layer after  $\text{POCl}_3$  annealing is summarized in figure 21. It is found that when the annealing temperature was in excess of  $950^\circ\text{C}$ , minority carrier lifetime can be increased to  $3 \mu\text{s}$  and saturated thereafter. The interface defect state density was then measured via the C-V method. The results showed that the interface defect state density decreased significantly when the  $\text{POCl}_3$  annealing temperature was above  $950^\circ\text{C}$ , and an evident consistency between the defect state density reduction and lifetime enhancement can be found. Further from the result of secondary ion mass spectroscopy measurement, Okuda *et al* [78] observed that P atoms were located at the SiC/ $\text{SiO}_2$  interface after  $\text{POCl}_3$  annealing at an appropriate temperature, which suggests that P atoms are most likely to terminate silicon or carbon dangling bonds.

## 6. Conclusion

In this paper, we review the typical surface defects in 4H-SiC material, their characterization methods, and various passivation schemes. In general, surface defects in 4H-SiC material include triangle defect, pit, carrot defect, and surface step. These defects are able to act as recombination centers, which lead to a decrease in the effective minority carrier lifetime. Furthermore, to better understand surface defects, it is essential to have methods to characterize them. At present,  $\mu$ -PCD, TRPL, SCM and C-AFM are the useful methods to characterize the recombination ability of various surface defects. In detail,  $\mu$ -PCD is able to provide an average lifetime of a specific surface defect whilst TRPL is able to reveal the size and shape of a specific surface defect.

Research on the deep level defects in 4H-SiC material demonstrates that the  $Z_{1/2}$  defect mainly controlled the minority carrier lifetime when its concentration exceeds  $10^{13} \text{cm}^{-3}$ . However, the minority carrier lifetime is controlled by the recombination at the surface defects when  $Z_{1/2}$  defect concentration was lower than  $10^{13} \text{cm}^{-3}$ . Surface defects act as non-radiative recombination channels and therefore cause a deterioration of minority carrier lifetime. To improve the surface quality of 4H-SiC material, surface defects need to be passivated. Nitridation and hydrogen passivation are feasible methods to passivate surface defects. In terms of the mechanism, forming Si-N and Si-H bonds are mainly responsible for the decline of surface dangling bonds at the 4H-SiC surface. Moreover, S passivation and P passivation are also demonstrated to be effective for the passivation of various surface defects in 4H-SiC material.

## Data availability statement

All data that support the findings of this study are included within the article (and any supplementary files).





## Acknowledgments

The authors would like to acknowledge the funding from the ‘Pioneer’ and ‘Leading Goose’ R&D Program of Zhejiang (2022C01021).

## Conflict of interest

The authors declare no conflict of interest.

## ORCID iDs

Can Cui  <https://orcid.org/0000-0002-8429-5875>  
 Naifu Zhang  <https://orcid.org/0000-0003-4137-3236>  
 Lihui Song  <https://orcid.org/0000-0001-5536-8388>  
 Xiaodong Pi  <https://orcid.org/0000-0002-4233-6181>

## References

- [1] Matsunami H and Kimoto T 1997 Step-controlled epitaxial growth of SiC: high quality homoepitaxy *Mater. Sci. Eng. R* **20** 125–66
- [2] Bergman P *et al* 2002 Characterisation and defects in silicon carbide *Mater. Sci. Forum* **389–393** 9–14
- [3] Sugawara Y, Takayama D *et al* 2004 12.7 kV ultra high voltage SiC commutated gate turn-off thyristor: SICGT *16th Int. Symp. on Power Semiconductor Devices and ICs* pp 365–8
- [4] Storasta L *et al* 2002 Electrical activity of residual boron in silicon carbide *Mater. Sci. Forum* **389–393** 549–52
- [5] Bergman J P, Kordina O and Janzén E 1997 Time resolved spectroscopy of defects in SiC *Phys. Status Solidi a* **162** 65–77
- [6] Zhang J, Storasta L, Bergman J P, Son N T and Janzén E 2003 Electrically active defects in n-type 4H-silicon carbide grown in a vertical hot-wall reactor *J. Appl. Phys.* **93** 4708–14

- [7] Klein P B, Shanabrook B V, Huh S W, Polyakov A Y, Skowronski M, Sumakeris J J and O'Loughlin M J 2006 Lifetime-limiting defects in n(-) 4H-SiC epilayers *Appl. Phys. Lett.* **88** 5
- [8] Danno K, Nakamura D and Kimoto T 2007 Investigation of carrier lifetime in 4H-SiC epilayers and lifetime control by electron irradiation *Appl. Phys. Lett.* **90** 20
- [9] Dalibor T, Pensl G, Matsunami H, Kimoto T, Choyke W J, Schöner A and Nordell N 1997 Deep defect centers in silicon carbide monitored with deep level transient spectroscopy *Phys. Status Solidi a* **162** 199–225
- [10] Hiyoshi T and Kimoto T 2009 Elimination of the major deep levels in n- and p-type 4H-SiC by two-step thermal treatment *Appl. Phys. Express* **2** 9
- [11] Kato M, Yoshida A and Ichimura M 2012 Estimation of surface recombination velocity from thickness dependence of carrier lifetime in n-type 4H-SiC epilayers *Jpn. J. Appl. Phys.* **51** 02BP12
- [12] Mori Y, Kato M and Ichimura M 2013 Estimation of surface recombination velocities for n-type 4H-SiC surfaces treated by various processes *15th Int. Conf. on Silicon Carbide and Related Materials (ICSCRM)* vol 778–780 pp 432–5
- [13] Mahadik N A, Stahlbush R E, Klein P B, Khachatryan A, Buchner S and Block S G 2017 Carrier lifetime variation in thick 4H-SiC epilayers using two-photon absorption *Appl. Phys. Lett.* **111** 22
- [14] Pennington G and Ashman C R 2007 Nitrogen passivation of (0001) 4H-SiC dangling bonds *12th Int. Conf. on Silicon Carbide and Related Materials* vol 600–603 pp 469–72
- [15] Ichikawa Y, Ichimura M, Kimoto T and Kato M 2018 Passivation of surface recombination at the Si-Face of 4H-SiC by acidic solutions *ECS J. Solid State Sci. Technol.* **7** 127–30
- [16] Su J, Yang Y, Zhang X, Wang H and Zhu L 2019 Sulfur passivation of 3C-SiC thin film *J. Cryst. Growth* **505** 15–18
- [17] Kimoto T 2016 Bulk and epitaxial growth of silicon carbide *Prog. Cryst. Growth Charact. Mater.* **62** 329–51
- [18] Picard Y N, Liu K X, Stahlbush R E, Twigg M E, Zhang X and Skowronski M 2008 Nondestructive dislocation delineation using topographically enhanced imaging of surface morphologies in 4H-SiC epitaxial layers *J. Appl. Phys.* **103** 7
- [19] Fujiwara H, Naruoka H, Konishi M, Hamada K, Katsuno T, Ishikawa T, Watanabe Y and Endo T 2012 Relationship between threading dislocation and leakage current in 4H-SiC diodes *Appl. Phys. Lett.* **100** 24
- [20] Fujiwara H, Naruoka H, Konishi M, Hamada K, Katsuno T, Ishikawa T, Watanabe Y and Endo T 2012 Impact of surface morphology above threading dislocations on leakage current in 4H-SiC diodes *Appl. Phys. Lett.* **101** 4
- [21] Zhang X, Nagano M and Tsuchida H 2010 Correlation between thermal stress and formation of interfacial dislocations during 4H-SiC epitaxy and thermal annealing *8th European Conf. on Silicon Carbide and Related Materials* vol 679–680 pp 306–9
- [22] Tsuchida H, Ito M, Kamata I and Nagano M 2009 Formation of extended defects in 4H-SiC epitaxial growth and development of a fast growth technique *Phys. Status Solidi b* **246** 1553–68
- [23] Hassan J, Henry A, McNally P J and Bergman J P 2010 Characterization of the carrot defect in 4H-SiC epitaxial layers *J. Cryst. Growth* **312** 1828–37
- [24] Ma P, Ni J J, Sun J, Zhang X, Li J and Chen H 2020 Three-dimensional detection and quantification of defects in SiC by optical coherence tomography *Appl. Opt.* **59** 1746–55
- [25] Guosheng S, Fei Y and Song B 2018 4H silicon carbide substrate and epitaxial layer defect map vol 11 p 20
- [26] Ishida Y, Takahashi T, Okumura H, Arai K and Yoshida S 2007 Origin of giant step bunching on 4H-SiC (0001) surfaces *12th Int. Conf. on Silicon Carbide and Related Materials* vol 600–603 p 473
- [27] Ishida Y and Yoshida S 2013 Simulation studies on giant step bunching accompanying trapezoid-shape defects in a 4H-SiC epitaxial layer *15th Int. Conf. on Silicon Carbide and Related Materials (ICSCRM)* vol 778–780 pp 222–5
- [28] Ishida Y and Yoshida S 2013 Simulation studies on giant step bunching in 4H-SiC epitaxial growth: cluster effect *15th Int. Conf. on Silicon Carbide and Related Materials (ICSCRM)* vol 778–780 pp 183–6
- [29] Matsuhata H, Sugiyama N, Chen B, Yamashita T, Hatakeyama T and Sekiguchi T 2017 Surface defects generated by intrinsic origins on 4H-SiC epitaxial wafers observed by scanning electron microscopy *Microscopy* **66** 95–102
- [30] Zhao L X 2020 Surface defects in 4H-SiC homoepitaxial layers *Nanotechnol. Precis. Eng.* **3** 229–34
- [31] Ogita Y I 1996 Bulk lifetime and surface recombination velocity measurement method in semiconductor wafers *J. Appl. Phys.* **79** 6954–60
- [32] Bachrach R Z and Lorimor O G 1972 Measurement of extrinsic room-temperature minority carrier lifetime in gap *J. Appl. Phys.* **43** 500
- [33] Wang K and Kampwerth H 2014 Separation algorithm for bulk lifetime and surface recombination velocity of thick silicon wafers and bricks via time-resolved photoluminescence decay *J. Appl. Phys.* **115** 173103
- [34] Giesecke J A, Kasemann M, Schubert M C, Würfel P and Warta W 2010 Separation of local bulk and surface recombination in crystalline silicon from luminescence reabsorption *Prog. Photovolt.* **18** 10–19
- [35] Kimura K, Kobayashi K, Yamada H and Matsushige K 2003 Two-dimensional dopant profiling by scanning capacitance force microscopy *Appl. Surf. Sci.* **210** 93–98
- [36] Barrett R C and Quate C F 1992 Large-scale charge storage by scanning capacitance microscopy *Ultramicroscopy* **42–44** 262–7
- [37] Pineda J P, Pascual G, Kim B and Lee K (available at: [www.parksystems.com/images/media/appnote/Electrical-Characterization-of-Semiconductor-Device-Using-SCM-and-KPFM-Imaging\\_8.pdf](http://www.parksystems.com/images/media/appnote/Electrical-Characterization-of-Semiconductor-Device-Using-SCM-and-KPFM-Imaging_8.pdf))
- [38] Suda J, Nakamura S-I, Miura M, Kimoto T and Matsunami H 2002 Scanning capacitance and spreading resistance microscopy of SiC multiple-pn-junction structure *Jpn. J. Appl. Phys.* **41** L40
- [39] Fiorenza P, Di Franco S, Giannazzo F and Roccaforte F 2016 Nanoscale probing of the lateral homogeneity of donors concentration in nitridated SiO<sub>2</sub>/4H-SiC interfaces *Nanotechnology* **27** 315701
- [40] Doi A, Nakajima M, Masuda S, Satoh N and Yamamoto H 2019 Cross-sectional observation in nanoscale for Si power MOSFET by atomic force microscopy/Kelvin probe force microscopy/scanning capacitance force microscopy *Jpn. J. Appl. Phys.* **58** S1A04
- [41] Fiorenza P, Alessandrino M S, Carbone B, Di Martino C, Russo A, Saggio M, Venuto C, Zanetti E, Giannazzo F and Roccaforte F 2020 Understanding the role of threading dislocations on 4H-SiC MOSFET breakdown under high temperature reverse bias stress *Nanotechnology* **31** 125203
- [42] Yang C H *et al* 2009 Electric modulation of conduction in multiferroic Ca-doped BiFeO<sub>3</sub> films *Nat. Mater.* **8** 485–93
- [43] Cheong L-Z, Zhao W, Song S and Shen C 2019 Lab on a tip: applications of functional atomic force microscopy for the study of electrical properties in biology *Acta Biomater.* **99** 33–52
- [44] Si H, Zhang S, Ma S, Xiong Z, Kausar A, Liao Q, Zhang Z, Sattar A, Kang Z and Zhang Y 2020 Emerging conductive

- atomic force microscopy for metal halide perovskite materials and solar cells *Adv. Energy Mater.* **10** 1903922
- [45] Peng J *et al* 2017 Interface passivation using ultrathin polymer–fullerene films for high-efficiency perovskite solar cells with negligible hysteresis *Energy Environ. Sci.* **10** 1792–800
- [46] Tu B *et al* 2019 Novel molecular doping mechanism for n-doping of SnO<sub>2</sub> via triphenylphosphine oxide and its effect on perovskite solar cells *Adv. Mater.* **31** 1805944
- [47] Eriksson J, Roccaforte F, Fiorenza P, Weng M-H, Giannazzo F, Lorenzi J, Jegenyes N, Ferro G and Raineri V 2011 Nanoscale probing of dielectric breakdown at SiO<sub>2</sub>/3C–SiC interfaces *J. Appl. Phys.* **109** 013707
- [48] Tawara T *et al* 2004 Evaluation of free carrier lifetime and deep levels of the thick 4H-SiC epilayers *Mater. Sci. Forum* **457–460** 565–8
- [49] Hemmingsson C G, Son N T, Ellison A, Zhang J and Janzén E 1998 Negative-U centers in 4H silicon carbide *Phys. Rev. B* **58** 10119–22
- [50] Dalibor T, Pensl G, Kimoto T, Matsunami H, Sridhara S, Devaty R P and Choyke W J 1997 Radiation-induced defect centers in 4H silicon carbide *Diam. Relat. Mater.* **6** 1333–7
- [51] Hemmingsson C, Son N T, Kordina O, Bergman J P, Janzén E, Lindström J L, Savage S and Nordell N 1997 Deep level defects in electron-irradiated 4 H SiC epitaxial layers *J. Appl. Phys.* **81** 6155–9
- [52] Reshanov S A, Bartsch W, Zippelius B and Pensl G 2008 Lifetime investigations of 4H-SiC pin power diodes *7th European Conf. on Silicon Carbide and Related Materials* vol 615–617 pp 699–702
- [53] Shockley W and Read W T 1952 Statistics of the recombinations of holes and electrons *Phys. Rev.* **87** 835–42
- [54] Hall R N 1952 Electron-hole recombination in germanium *Phys. Rev.* **87** 387
- [55] Klein P B, Myers-Ward R, Lew K-K, VanMil B L, Eddy C R, Gaskill D K, Shrivastava A and Sudarshan T S 2010 Recombination processes controlling the carrier lifetime in n(-)4H-SiC epilayers with low Z(1/2) concentrations *J. Appl. Phys.* **108** 3
- [56] Kimoto T, Hiyoshi T, Hayashi T and Suda J 2010 Impacts of recombination at the surface and in the substrate on carrier lifetimes of n-type 4H-SiC epilayers *J. Appl. Phys.* **108** 8
- [57] Sridhara S G, Carlsson F H C, Bergman J P and Janzén E 2001 Luminescence from stacking faults in 4 H SiC *Appl. Phys. Lett.* **79** 24
- [58] Tabib-Azar M, Hubbard S M, Schnabel C M and Bailey S 1998 Mapping of crystal defects and the minority carrier diffusion length in 6H-SiC using a novel electron beam induced current technique *J. Appl. Phys.* **84** 7
- [59] Niu Y-X, Tang X-Y, Jia R-X, Sang L, Hu J-C, Yang F, Wu J-M, Pan Y and Zhang Y-M 2018 Influence of triangle structure defect on the carrier lifetime of the 4H-SiC ultra-thick epilayer *Chin. Phys. Lett.* **35** 077103
- [60] Hassan J and Bergman J P 2009 Influence of structural defects on carrier lifetime in 4H-SiC epitaxial layers: optical lifetime mapping *J. Appl. Phys.* **105** 12
- [61] Chung G Y, Tin C C, Williams J R, McDonald K, Di Ventra M, Pantelides S T, Feldman L C and Weller R A 2000 Effect of nitric oxide annealing on the interface trap densities near the band edges in the 4H polytype of silicon carbide *Appl. Phys. Lett.* **76** 1713–5
- [62] Schorner R, Friedrichs P, Peters D, Stephani D, Dimitrijević S and Jamet P 2002 Enhanced channel mobility of 4H-SiC metal-oxide-semiconductor transistors fabricated with standard polycrystalline silicon technology and gate-oxide nitridation *Appl. Phys. Lett.* **80** 4253–5
- [63] Jamet P *et al* 2002 Passivation of the oxide/4H-SiC interface *Mater. Sci. Forum* **389–393** 973–6
- [64] Akiyama T, Shimizu T, Ito T, Kageshima H, Chokawa K and Shiraishi K 2022 *Ab initio* study for orientation dependence of nitrogen incorporation at 4H-SiC/SiO<sub>2</sub> interfaces *Jpn. J. Appl. Phys.* **61** SH1002
- [65] Kimoto T, Nanen Y, Hayashi T and Suda J 2010 Enhancement of carrier lifetimes in n-type 4H-SiC epitaxial layers by improved surface passivation *Appl. Phys. Express* **3** 12
- [66] Noborio M, Suda J, Beljakova S, Krieger M and Kimoto T 2009 4H-SiC MISFETs with nitrogen-containing insulators *Phys. Status Solidi a* **206** 2374–90
- [67] Higashi G S, Chabal Y J, Trucks G W and Raghavachari K 1990 Ideal hydrogen termination of the Si-(111) surface *Appl. Phys. Lett.* **56** 656–8
- [68] Graf D, Grundner M, Schulz R and Mühlhoff L 1990 Oxidation of HF-treated Si wafer surfaces in air *J. Appl. Phys.* **68** 5155–61
- [69] Nauka K and Kamins T I 1999 Surface photovoltage measurement of hydrogen-treated Si surfaces *J. Electrochem. Soc.* **146** 292–5
- [70] Coletti C, Frewin C L, Hoff A M and Sadow S E 2008 Electronic passivation of 3C-SiC(001) via hydrogen treatment *Electrochem. Solid State Lett.* **11** H285–7
- [71] Seyller T 2006 Electronic properties of SiC surfaces and interfaces: some fundamental and technological aspects *Appl. Phys. A* **85** 371–85
- [72] Sieber N, Seyller T, Ley L, James D, Riley J D, Leckey R C G and Polcik M 2003 Synchrotron x-ray photoelectron spectroscopy study of hydrogen-terminated 6H-SiC{0001} surfaces *Phys. Rev. B* **67** 20
- [73] Tsuchida H, Kamata I and Izumi K 1999 Infrared attenuated total reflection spectroscopy of 6H-SiC(0001) and (000(1) over-bar)surfaces *J. Appl. Phys.* **85** 3569–75
- [74] Starke U 1997 Atomic structure of hexagonal SiC surfaces *Phys. Status Solidi b* **202** 475–99
- [75] Lin M E, Strite S, Agarwal A, Salvador A, Zhou G L, Teraguchi N, Rockett A and Morkoç H 1993 GAN grown on hydrogen plasma cleaned 6H-SiC substrates *Appl. Phys. Lett.* **62** 702–4
- [76] van Elsbergen V, Janzen O and Mönch W 1997 Oxidation of clean and H-terminated SiC surfaces *Mater. Sci. Eng. B* **46** 366–9
- [77] Zhang R *et al* (eds) 2021 The influence of hydrogen annealing on minority carrier lifetimes in 4H-SiC *2021 IEEE Workshop on Wide Bandgap Power Devices and Applications in Asia (WiPDA Asia)* (August 2021) pp 25–27
- [78] Okuda T, Kobayashi T, Kimoto T and Suda J 2016 Surface passivation on 4H-SiC epitaxial layers by SiO<sub>2</sub> with POCl<sub>3</sub> annealing *Appl. Phys. Express* **9** 5